Electrical Properties of Graphene Polymer Nanocomposites

P. Noorunnisa Khanam, Deepalekshmi Ponnamma and M.A. AL-Madeed

Abstract Graphene, a monolayer of sp^2 hybridized carbon atoms arranged in a two dimensional lattice has attracted electronic industrial interest due to its exceptional electrical properties. One of the most promising applications of this material is in polymer nanocomposites in which the interface of graphene based materials and polymer chains merge to develop the most technologically promising devices. This chapter presents the electrical properties of such graphene based polymer nanocomposites and also discusses the effect of various factors on their electrical conductivity. Graphene enables the insulator to conductor transition at significantly lower loading by providing percolated pathways for electron transfer and making the polymers composite electrically conductive. The effect of processing conditions, dispersion, aggregation, modification and aspect ratio of graphene on the electrical conductivity of the graphene/polymer nanocomposites is conferred.

Keywords Conductivity · Percolation · Filler modification · Volume fraction · Fabrication

1 Introduction

Graphene, a two-dimensional, single-atom-thick structure of sp^2 bonded carbon atoms, has attracted tremendous research interest due to their excellent reinforcement, electrical properties, unique physical characteristics and high mechanical properties. Therefore, recent research has focused on developing high performance polymer nanocomposites, with the benefit of graphene nanotechnology, to

P.N. Khanam (✉) · M.A. AL-Madeed
Centre for Advanced Materials, Qatar University, Doha, Qatar
e-mail: noor.pathan@qu.edu.qa; pnkhanam_phd@yahoo.com

D. Ponnamma
School of Chemical Sciences, Mahatma Gandhi University, Kottayam 686560, Kerala, India

achieve novel composite materials for a wide range of industrial fields. Graphene dramatically improves the properties of polymer based composites at a very low loading and its most fascinating property is the very high surface conductivity leading to the formation of numerous electrically conductive polymer composites. Such conducting graphene nanocomposites have been widely applied in anti-static materials, electromagnetic interference (EMI) shielding, chemical sensor, bipolar plates for fuel cells etc. Other possible applications include radio-frequency interference shielding for electronic devices and electrostatic dissipation [1–3].

By using conventional processing methods, graphene composites can be easily fabricated into intricately shaped components with excellent preservation of the structure and properties. This is very important to make full use of the outstanding properties of graphene. Compared with carbon nanotubes (CNTs), graphene has a higher surface-to-volume ratio because of the inaccessibility of the CNT's inner tube surface to polymer molecules. This makes graphene potentially more favorable for improving the properties of polymer matrices, such as electrical properties. Therefore, graphene-based polymer composites have attracted both academic and industrial interest [3].

The present chapter gives an overview of the electrical properties of graphene based polymer nanocomposites. A brief description about the synthesis and characterization of graphene is also included in this chapter. Since the present book deals with the applications of graphene nanocomposites in various fields of flexible and wearable electronics, we think this chapter is of much significance as electrical conductivity is the basis for graphene's such applications. After giving an outline about the electrical properties of graphene polymer composites, the various factors affecting the conductivity such as filler aspect ratio, dispersion, modification of graphene surfaces etc. are also discussed here. The phenomenon of percolation threshold is also well pictured and finally this chapter ends with a few applications.

## 2 Synthesis and Characterization

2.1 Synthesis of Graphene

Graphite is available in large quantities as in the form of both natural and synthetic sources and is rather inexpensive [4]. The main graphite derivatives include EG, graphite oxide, graphene nanoplatelets (GNP), graphene oxide (GO), reduced graphene oxide (RGO), and graphene. Because the electronic, photonic, mechanical, and thermal properties of graphene depend on the number of layers [5] [although the monolayer (ML), bi-layer (BL), and tri-layer (TL) graphenes have practical significance] and its crystalline structure, the controlled synthesis of graphene with defined layers is rather significant. The mechanical peeling method by which graphene is first produced [6] is not used for an industrial scale of production. The GO and RGO derivatives are usually synthesized via solution-based oxidation and reduction by thermal and chemical methods, whereas graphene layers with

superior electron transport characteristics are always synthesized using dry methods such as chemical vapor deposition (CVD) and surface segregation [6–13]. Although more than 95 % of graphene has been grown on Cu foil [5], this growth was not epitaxial, and thus complete growth over the entire substrate remains a major challenge. The surface of Ni(III) proved to be the best substrate for the epitaxial growth of structurally homogeneous graphene due to the small lattice mismatch of this surface with that of graphene and highly oriented pyrolytic graphite [14]. However, this method suffers from the disadvantage of carbon solubility in nickel, and thus achieving uniform thickness throughout the substrate is difficult. The simple method of surface segregation [15–17] was recently introduced to solve this problem and to epitaxially grow graphene over Ni film (~100 nm thick) [18]. Raman spectroscopy and scanning tunneling microscopy (STM) verified the homogeneity of the graphene layer over the entire Ni film [19–21].

2.2 Preparation of Graphene Polymer Composites

Various preparation methods employed to synthesize graphitic filler reinforced polymer nanocomposites include melt mixing, solution mixing and in situ polymerization. In addition to these three traditional polymer composite preparation methods, many other methods are also practiced for material fabrication. Since the common methods were the subjects for several reviews, a few other methods are introduced here. In a typical tape casting method [22], a mixture of natural flake graphite powders (NGP) and polyvinyl butyral (PVB) is stirred magnetically in ethanol, and after removing air bubbles by evacuation, this mixture is casted on a plastic film using a blade, as shown in Fig. 1a. The blade imparts a shearing force that orients the composite containing anisotropic graphite particles. This method was tested by varying the concentration of graphite powders from 10 to 95 wt% and varying the blade heights from 300 to 500 μm. A narrow blade gap is essential for producing a strong shearing force for better orientation, and the different testing conditions also affect thermal conductivity as well as the degrees of orientation [23].
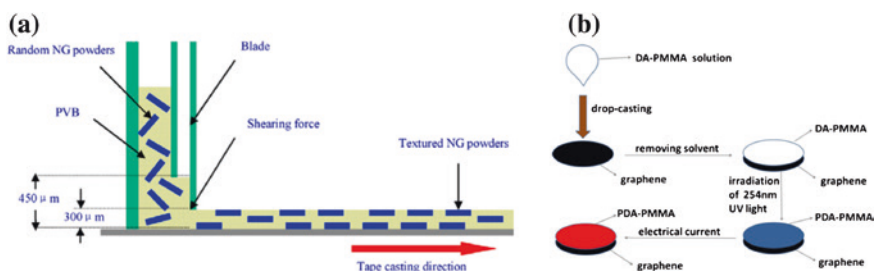

Fig. 1 Schematic of **a** tape-casting process and **b** electrochromic process [22]. Copyright 2012. Reproduced with permission from Elsevier Ltd. [24]. Copyright 2013. Reproduced with permission from American Chemical Society

In another preparation process, polydiacetylene (PDA)-Polymethylmethacrylate (PMMA)/graphene composites were developed that are capable of responding to electrical current with a color change. In the so-called electrochromic method (Fig. 1b), PDA acts as the electrochromic material and the graphene provides conductivity. The PMMA serves as the inert polymer matrix and improves the mechanical properties and colorimetric phenomenon. The blue-red phase transition is clearly visible in PDA-PMMA/graphene compared with that of PDA/graphene. The critical current for the color transition can be varied with the amount of graphene [24].

Mixing of functionalized GO with epoxy resin by sonication transfers the modified GO particles from the water to the epoxy. This is yet another fabrication method practiced. After decanting the water, heating the mixture forms a dark violet epoxy-modified GO composite, and the epoxy can be cured by adding hardener. The calculated volume fractions of functionalized GO in the final composites were 1.16 and 2.2 g/cm^3, respectively [25]. Copper oxide nanoparticle/graphene (CuO-GR) nanocomposites were prepared using GO synthesized by Hummers method. The copper-acetate-adsorbed GO acts as a precursor. The GO was washed with de-ionized water to remove the remaining metal ions and acid, and a copper(II) nitrate aqueous solution was added. Again, ammonium hydroxide was added under magnetic stirring, and the mixture was transferred to an autoclave at 100 °C. The black CuO-GR nanocomposites formed were washed with distilled water and ethanol [26].

## 2.3 Characterization of Polymer Nanocomposites

Many important characteristic techniques reveal the morphology, structure and superior properties of graphitic fillers and their polymer composites. Of the various characterization techniques, three important methods of analysis for the materials are explained in this section- X-ray diffraction spectroscopy (XRD), Fourier Transformation Infrared (FTIR) Spectroscopy and Raman spectroscopy. Figure 2 shows the XRD pattern for the graphite, GO and their mode of dispersion in polyaniline (PANI). Using the peak observed at 2θ/10.04°, the GO grain size was estimated as 5.1 nm. In the case of a polymer, the crystallized PANI gives a broad band extending from 15° to 34° [27]. For the PANI composite, the intensity of the peak at 10.04° is affected (Fig. 2a) [28]. Variation in the XRD spectrum is also observed for PDA composites prepared under different temperature conditions because of the influence of experimental conditions on the exfoliation rate of RGO fillers [28]. The peak centered at 26° corresponding to the (002) plane of graphite [29] is observed in Fig. 2b [30]. EG also shows the same peak, whereas for GO, the diffraction peak is shifted to 9.8° corresponding to a *d*-spacing of 0.9 nm [30]. The weak diffraction maximum of EG compared to graphite is attributed to its exfoliated nature. In GO, the *d*-spacing depends on the method of preparation and the number of layers of water trapped in the structure of the material
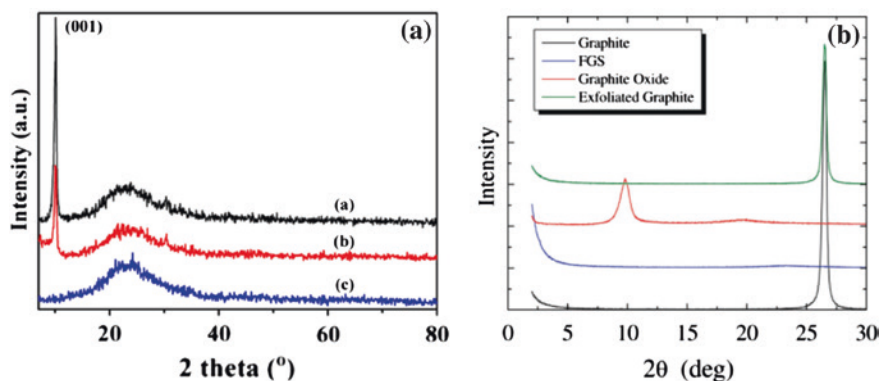
Fig. 2 **a** XRD patterns of the *a* GO film, *b* PANI/GO nanocomposite film, and *c* PANI film [28]. Copyright 2013. Reproduced with permission from Elsevier Ltd. **b** XRD Pattern of FGS, GO, and EG [30]. Copyright 2009. Reproduced with permission from John Wiley & Sons

[30]. Functionalised graphene sheets (FGS) show no characteristic peak indicating the loss of long-range stacking order in the material. Also in the graphene case, the Bragg peak is totally absent because pure graphene contains no stacks.

Another important characterization tool is FTIR, which confirms the chemical structure of nanocomposites and interactions among them. The FTIR spectra obtained for graphite, GO, magnetite–graphene (MG), and Pd/Fe_3O_4/graphene (PMG) nanocomposites are shown in Fig. 3 [31]. In GO, the presence of different
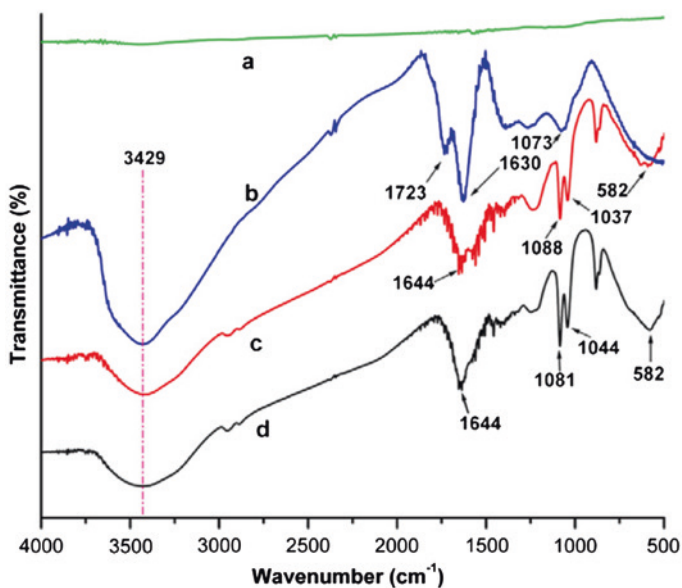

Fig. 3 FTIR spectra of **a** graphite, **b** GO, **c** MG and **d** PMG nanocomposite [31]. Copyright 2012. Reproduced with permission from Elsevier Ltd.

types of oxygen functionalities are confirmed as evidenced from the bands at 3,429, 1,723, 1,630, 1,618 and 1,073 cm^{-1} corresponding to the O–H groups, $C = O$ carbonyl/carboxyl groups, $C = C$ aromatic groups and C–O in the epoxide group, respectively [31, 32]. As a result GO interacts with metal ions and the additional peak at 582 cm^{-1} in MG and PMG composites implies the formation of Fe–O bond. The two additional peaks at 1,037 and 1,088 cm^{-1} for MG and at 1,044 cm^{-1} for PMG corresponds to distinct C–O stretching vibrations, involving the formation of metal nanoparticles by binding C–O with different metal ions [31].

In general RGO, the intensity of the O–H band at 3,430 cm^{-1} was reduced due to the de-oxygenation of the GO functionalities. For the RGO-(PMMA) nanocomposites obtained from the in situ method, the bands present at 3,420, 1,726 and 1,620 cm^{-1} are due to the presence of O–H, $C = O$ and $C = C$ groups, respectively [33]. When GO-PMMA is reduced in the case of R-(GO-PMMA), the intensity of the $C = C$ bands increases, whereas that of the $C = O$ band decreases.

The best technique for discriminating graphite and graphene is Raman spectroscopy, which is explained with the aid of Figs. 4, 5, and 6 [34–36]. This simple spectroscopy technique is capable of identifying the number of graphene layers, orientation and crystalline quality of the graphene layers [5, 37]. Figure 4a [34] shows the typical Raman signals of graphene recovered from dispersions of 3-glycidoxypropyl trimethoxysilane (GPTMS) and phenyl triethoxysilane (PhTES), and both are similar. In particular, graphene obtained from PhTES exhibits a G band at 1,577 cm^{-1}, a 2D band at 2,696 cm^{-1}, and a D peak at 1,346 cm^{-1}, whereas for the other graphene obtained from GPTMS, the G band is located at 1,574 cm^{-1}, the 2D band at 2,701 cm^{-1}, and the D band at 1,345 cm^{-1}. The 2D bands are de-convoluted in Fig. 4b [34], and the components of the 2,701 cm^{-1} peak resemble those of bilayer graphene [38]. The 2D peak of graphite consists of two components, and the main peak is upshifted to 2,713 cm^{-1}.
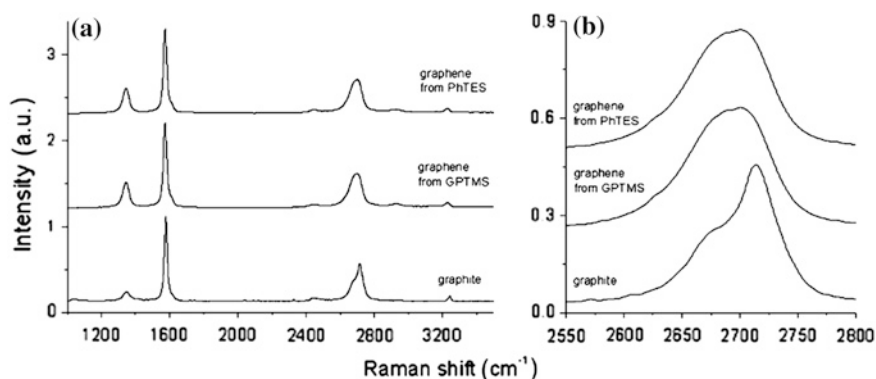
Fig. 4 Raman spectra of graphene obtained by sonication in PhTES and GPTMS from 5 wt% of the initial graphite compared with graphite (**a**) 2D peaks evaluation for this systems (**b**) [34]. Copyright 2009. Reproduced with permission from Springer
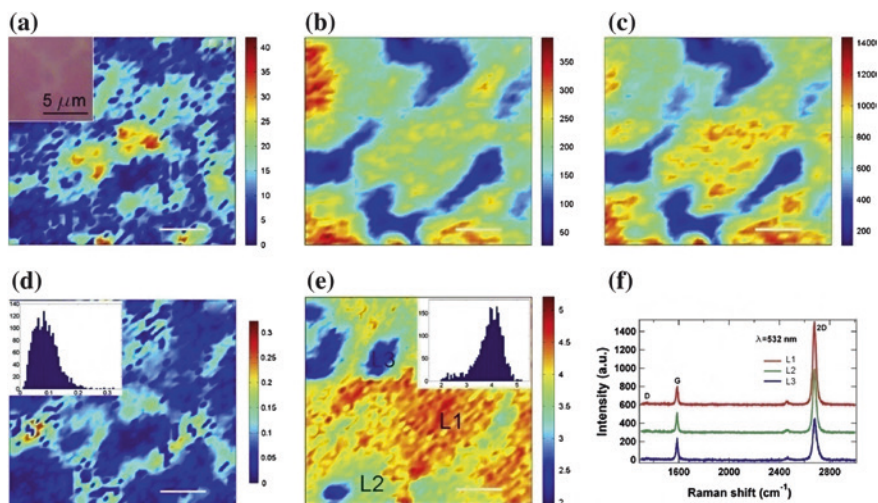
Fig. 5 Raman characterization of CVD graphene. All Raman maps for I_D (**a**), I_G (**b**), I_{2D} (**c**), I_D/I_G (**d**), and I_{2D}/I_G. In the histograms, x-axis indicates the ratios of I_D/I_G and I_{2D}/I_G and y-axis indicates counts. All of scale bars in maps are 2 μm, except (**a**) inset. Raman spectra shown in (**f**) measured from the marked location L1, L2 and L3 in (**e**), respectively. The D, G, and 2D bands are labeled in the spectra [35]. Copyright 2010. Reproduced with permission from Elsevier Ltd.

Spatially resolved Raman measurements on the CVD graphene films from a SiO$_2$/Si substrate were collected to probe the sample uniformity. A Raman map showing the intensity of the D, G and 2D bands measured in a 100 m^2 area of the CVD graphene sample is presented in Fig. 5a–c [35]. The insets of Fig. 5a, d and e [35] correspond to the optical microscope images of the scanned area and the histograms of I_D/I_G and I_{2D}/I_G. The data are fitted with Lorentzian formula, and the intensity of a given band is determined in terms of the amplitude value of the Lorentzian function fit. For fitting of the range, the D, G, and 2D bands were considered at 1,320–1,380, 1,560–1,620 and 2,640–2,720 cm^{-1} intervals.

From Fig. 5a–c [35], it is clear that the intensity maps of the G and 2D bands are correlated, whereas the D band is not. This occurs because the spatially non-uniform adhesion of transferred graphene causes the high-density locations of the G and 2D bands to be the same and also affects the intensity of the Raman spectra. It is noteworthy that the D band is always low, indicating the high quality of the graphene [5, 39]. The Raman map of I_D/I_G of the same scanned area is given in Fig. 5d [35]. In this figure, the $I_D/I_G < 0.1$ again confirms the low defect density in the graphene.

From Fig. 5 [35], for most of the mapped area, the value of $I_{2D}/I_G > 2$ indicates monolayer graphene. Additionally, as shown in Fig. 5f [35] from the corresponding marked spots in Fig. 5e [35], substantial variations from $I_{2D}/I_G > 2$ are observed at monolayer locations. This observation and notably large $I_{2D}/I_G > 5$ values are the reasons for spatially non-uniform adhesion between the graphene film and the

Fig. 6 Raman spectra of
graphene before buckling on
SiO$_2$/Si and after buckling on
PDMS. The *vertical arrows*
in the inset indicate the
expected 2D band position
($\sim$2,700 cm^{-1}) change [36].
Copyright 2011. Reproduced
with permission from
American Chemical Society
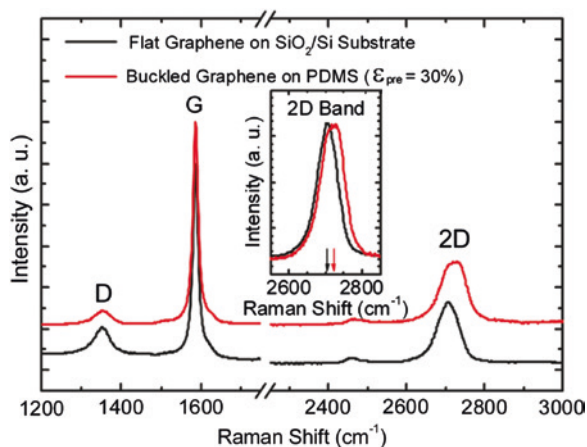
underlying SiO$_2$ substrate [40]. The adhesion can significantly affect the G and
1D band but to different extents. Quantum Hall measurements also support the
presence of monolayer graphene [41]. In short, Fig. 5 provides information on the
high quality and uniform monolayers of CVD-grown graphene films.

The Raman spectra of graphene on a SiO$_2$/Si substrate (black curve) and
buckled on PDMS (with a pre-strain of 30 %; red curve) are illustrated on Fig. 6
[36]. Due to the difference in the elastic moduli of graphene and PDMS, graphene
ripples are spontaneously formed during pre-strain release. During buckling,
compressive strain occurs in the graphene basal plane in addition to a geometry
change. The spectra are obtained by subtracting the PDMS substrate Raman signal
(red in figure). The D or 2D bands of graphene are quite sensitive to strain [42, 43]
and the absence of any obvious variations in either the G and D peak positions or
the I2D/IG ratios after many stretch-and-release cycles indicates that the defects
of the graphene ribbons are independent of the buckling process. However, a blue
shift of 15 cm^{-1} for the 2D peak is observed for graphene on PDMS compared
with that on SiO$_2$/Si. This observation goes against the observation reported by
Mohiuddin et al. [44] in which blue shifts were noted for both the G and 2D peaks
for graphene formed on PMMA. Because the shift in the G band is affected only
by doping, the shift in the 2D peak is the only parameter for estimating uniaxial
strain in the Raman measurements. This uniaxial strain can be quantified as well.

3 Electrical Conductivity and Percolation Threshold in Graphene Polymer Nanocomposites

Superior electrical conductivity is the most important property of graphene. When
graphene fills the insulating polymer matrix, conductive polymer composites result.
Various polymers, including PMMA, PVA, PVC, PP, PE, PA12, PS etc. [45, 46]

have been used as matrices to prepare electrically conductive graphene/polymer composites. Such composite materials generally exhibit a non-linear increase of the electrical conductivity as a function of the filler concentration. The two parameters, electrical conductivity and percolation threshold are together associated with. At a certain filler loading fraction, which is known as the percolation threshold (p_c), the fillers form a network leading to a sudden rise in the electrical conductivity of the composites [45, 46]. Sometimes addition of a very low amount of conducting particles can make filler contact to form effective conducting paths and thus making the whole composite conductive.

   A theoretical study by Xie et al. [47] predicted that graphene is more effective for conductivity improvement than competing nanofillers such as CNTs because of their large specific surface area. An outstanding electrically conductive graphene/polymer composite is expected to have lower percolation threshold and higher conductivity at a lower graphene loading, which can not only decrease the cost of filler but also preserve the processability of the composite. Ruoff et al. [48] synthesized graphene/PS composites and they observed a low percolation threshold at 0.1 vol% of graphene. The electrical conductivity variation in composites occurs in three stages, as illustrated in Fig. 7. Here the process is explained with a Graphene filled polymer. At first, the conductivity is quite low (Fig. 7a) due to a smaller number of additives, but large clusters gradually begin to form (Fig. 7b) with a slight increase in conductivity. At this stage, tunneling effects occur between neighboring graphene flakes, making it useful in Sensing materials.
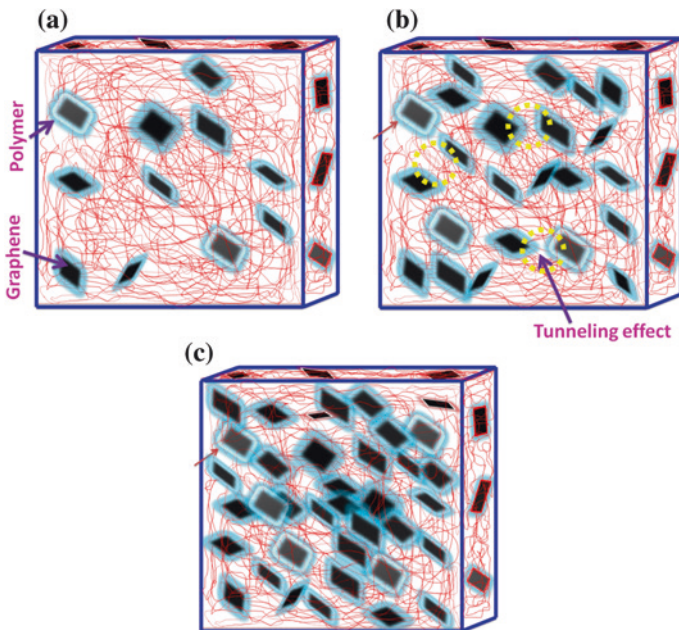

Fig. 7 Percolation process in conductive composites

As the graphene flakes increases, a complete conductive path (red) is formed by the contacting flakes (Fig. 7c) at the percolation, and further increase in the conducting particles enhances the number of conducting networks, as shown in Fig. 7c, until the conductivity levels off [49].

This explanation based on the way those nanoparticles form conducting network when dispersed in polymer matrix is called percolation theory. Various factors influence the electrical conductivity and the percolation threshold of the composites such as concentration of filler, aggregation of filler, processing methods, functionalization and aspect ratio of graphene sheets, inter-sheet junction, distribution in the matrix, wrinkles and folds etc. A more detailed study of these factors is done in the subsequent sections.

3.1 Effect of Graphene Concentration

In nanocomposites containing conducting fillers conduction takes place via tunneling between the thin polymer layers surrounding the filler particles, and this tunneling resistance is said to be the limiting factor in the composite conductivity. So in order to get a current flow in the composite, the direct contact between the filler is not necessary. However percolation of filler particles occurs and this enhances the electrical conductivity. The concentration of the filler for creating the percolation threshold varies from polymer to polymer. For instance Liang et al. reported a very low percolation threshold of 0.1 vol% for the solution-processable functionalized graphene filled epoxy composites compared to the percolation of 0.53 vol% for the neat graphene/epoxy nanocomposite [50]. For the graphene/ultra high molecular weight polyethylene composite, the percolation threshold was 0.070 vol% [51]. The graphene/polyethylene terephthalate (PET) nanocomposite [52] fabricated by melt compounding exhibited a percolation at 0.47 vol%. Kim et al. [53] reported lower percolation threshold of <0.5 vol% for TRGO while >2.7 vol% for graphite.

The synergy between MWCNTs and GNPs is successfully used to fabricate their polystyrene (PS) composites exhibiting a good response in terms of its DC conductivity value. Figure 8 illustrates the room temperature conductivity of PS/MWCNT/GNP nanocomposites prepared by in situ suspension polymerization of PS−GNP beads (50, 60 and 70 wt%) and MWCNT (0.1, 0.2 and 0.3 wt%). The increase in weight percent of both PS−GNP beads increased the conductivity of the composites, as shown in the figure [54].

The maximum electrical conductivity of $\sim 9.47 \times 10^{-3}$ S cm^{-1} is obtained in the case of PS–GNP (70 wt%) beads polymerized with 30 wt% PS-MWCNT containing 0.3 wt% MWCNT loading. Similar to the previous case, PS/MWCNT without PS–GNP beads was non-conducting with a 0.1 wt% loading of MWCNT. However, in situ polymerization of styrene−MWCNT in the presence of 50 wt% PS–GNP showed a conductivity value of $\sim 8.26 \times 10^{-7}$ S cm^{-1}. The MWCNT concentration in the in situ polymerized PS increases if PS−GNP is present and
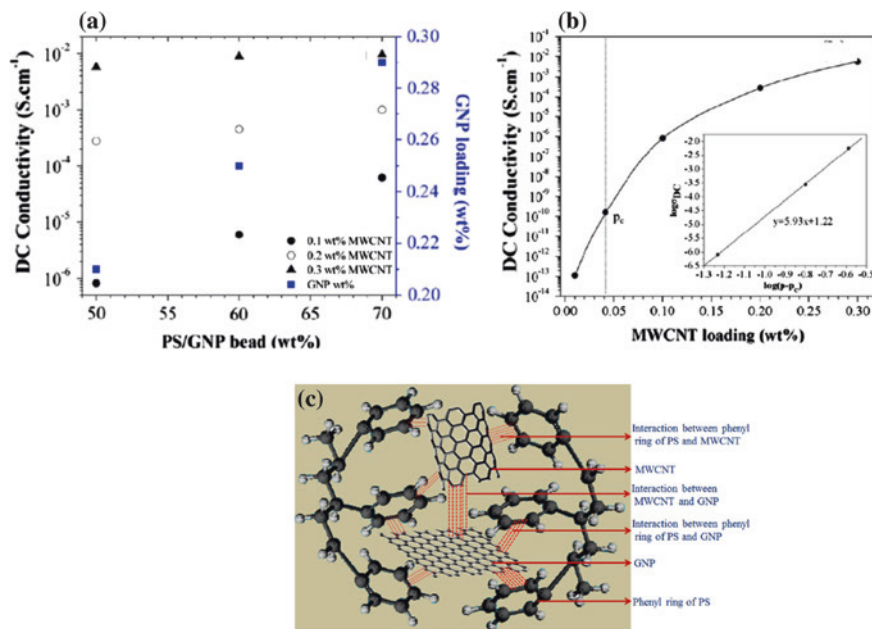
Fig. 8 DC conductivity of PS/MWCNT/GNP nanocomposites (**a**) at different wt% of PS–GNP beads and GNP loading with various MWCNT loadings (**b**) with MWCNT loading. (inset) log–log plot of σ_{DC} versus $(p–p_c)$ for the nanocomposites. *Straight line* in the inset is the model fit with the values $p_c = 0.041$ and $t = 5.93$. **c** Schematic representation shows $\pi–\pi$ interactions between GNP, MWCNT, and PS in the composites [54]. Copyright 2013. Reproduced with permission from American Chemical Society

thus develops a continuous GNP−CNT−GNP conductive network path. These interactions that occur in the composite are schematically shown in Fig. 8c [54], where the $\pi–\pi$ interaction between the phenyl rings of the PS and GNP sheets and the MWCNT is clear. For the excluded volume of PS–GNP beads in PS, the stick-like MWCNTs cannot enter, and thus the concentration of MWCNT will be high in the region of the in situ polymerized continuous PS phase adjoining the PS–GNP beads. These continuous GNP–CNT–GNP conductive network paths and $\pi–\pi$ interactions with PS throughout the matrix cause the DC conductivity to enhance. In the case of PET/graphene composites electrical conductivity increases rapidly to 7.4×10^{-2} S m^{-1} from 2.0×10^{-13} S m^{-1} with a slight increase in graphene content from 0.47 to 12 vol%. Here the percolation of the graphene filled composites was achieved at a 2.4 % loading [55]. At this filler concentration PET/graphene exhibits higher increment in electrical conductivity compared to PET/graphite composites.

Yue et al. [56] prepared epoxy/GNP/CNT hybrid composites at different mixing ratios by dissolving the fillers in the epoxy resin using simultaneous magnetic stirring and sonication in warm bath. The electrical conductivity studies for the composites with different filler content reported a percolation threshold of about

0.84 % for the CNT and 0.88 wt% for the GNP single filler epoxy composites. At 4 wt% the GNP/epoxy nanocomposite shows an electrical conductivity of 2.1×10^{-5} S m^{-1} which is almost 7 times the conductivity of neat epoxy. This substantiates GNP's excellent capacity in conduction at low concentration and good conductivity network was formed for both filler systems at low filler concentration. Low percolation threshold of graphene is also observed at 0.1 vol% for PS/graphene composites [48]. Moreover in RGO filled PVC/vinyl acetate copolymer composite and in PET composite the percolation values were 0.15 and 0.47 vol% respectively [46]. This is concluded to be due to the large surface area of graphene and also filler/matrix interaction mediated by surface functional groups of graphene which has a moderate role in this operation.

3.2 Effect of Fabrication Process

The mode of synthesis of graphene filled composites influence the filler distribution within the polymer matrix and thus regulate the electrical conductivity. It is reported that the electrical conductivity is higher for in situ polymerized and solvent blended samples than melt blended at the same filler volume fraction. This indicates better dispersion from solvent based strategies [46]. However the conductivity observed for melt processed samples is attributed to the annealing happened during the process by which particles disorient and regain contacts between one another.

The static and electrical conductivity of the polyvinylidene difluoride (PVDF) composites containing two different fillers, solvothermally reduced graphene (SRG) and RGO were checked and a lower percolation threshold was observed for the SRG/PVDF composites [57, 58] compared to the graphene/PVDF composite prepared by direct blending of chemically/thermally reduced GO sheets with polymers [59]. In the composite [57] the SRG sheets were homogeneously dispersed, which is attributed to the low p_c value. Additionally, the SRGs remain stable in the PVDF solution for weeks, whereas without PVDF, they precipitate in dymethyl formamide (DMF) after 1 day. During the fabrication step of the solvothermal process, the GO sheets enclosed by the PVDF chains were reduced and did not fold easily or form aggregates. This behavior facilitated the formation of a conducting network and resulted in a low percolation threshold. The large aspect ratios of the SRGs make the percolation threshold even smaller and its value calculated mathematically yield a percolation value at 0.31 vol%. Equation 1 gives the mathematical formula used for calculating the percolation threshold.

$$\sigma(p) = \sigma_0(P - P_0)^t, \ \ \text{for } P > P_c \tag{1}$$

where p_c is the percolation threshold, p is the filler content, and t is the critical exponent.

It is found that at 2.2 wt% RGO, the electrical conductivity of the RGO-filled PVDF increases enormously to 0.04 S m^{-1}, which is 14 orders of magnitude higher than that of neat PVDF. However at high concentrations of RGO, conductivity was notably low due to poor dispersion of the nanofiller in the polymer.

Fig. 9 Logarithm of the DC electrical conductivity versus EG concentration for the fast (FC) and slow (SC) cooled nanocomposites. *Continuous lines* are the predictions of percolation theory [27]. Copyright 2012. Reproduced with permission from John Wiley & Sons
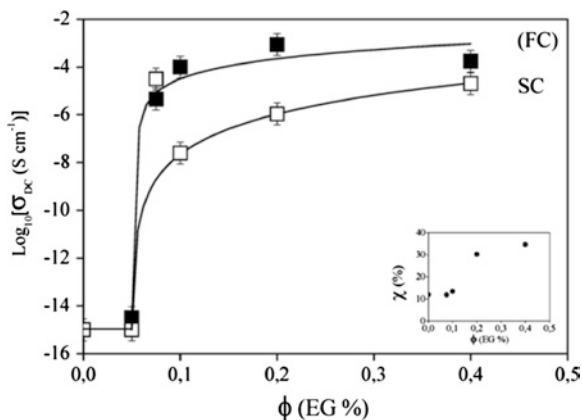
Once percolation is achieved, the RGO-PVDF shows high conductivity, and this material finds many electrical applications. The electrical conductivities of the RGO-PVDF composite again increase with the amount of RGOs due to the above-mentioned conductivity and percolation effects. He et al. [57] reported a very low percolation threshold of 0.31 vol% for the chemically reduced GO filled PVDF prepared by direct blending, which is lower than that of graphene/PVDF composites due to the homogeneous graphene dispersion achieved in the former case.

The electrical conductivity of fast- and slow-cooled nanocomposites containing EG is shown in Fig. 9 [27]. The slow-cooled sample containing 0.075 wt% EG was excluded from the continuous line fit (according to Eq. 1). This sample with 0.075 wt% EG exhibited the highest conductivity of all the nanocomposites and therefore was not considered in the fitting. Additionally, the values calculated for the fast-cooled nanocomposites were well within the expectations of the percolation theory, whereas those for the slow-cooled case were much greater. The surface resistivity of a material is the electrical resistance to a leakage current along the surface of the insulator and the effect of GNS filler on the surface resistivity of unsaturated polyester resin (UPR) nanocomposites is reported. It is found that the surface resistivity decreases with increase in the concentration of GNS due to the platelet structure, the larger surface area of GNS and the larger free path available within the polymer matrix for the free electrons to propagate. The surface resistivity value varies between $0.99 \times 1{,}015$ and $0.14 \times 1{,}015 \ \Omega$ cm from 0.01 to 0.1 concentrations of GNS.

The PS/GNS composite prepared using in situ emulsion polymerization showed and electrical conductivity of $\sim 2.9 \times 10^{-2}$ S m^{-1} at 2.0 wt% of GNS [60]. The higher conductivity occurred here is attributed to the compatibility between the PS microspheres and GNS which is sufficient to obtain nanosized dispersions without any additional surface treatment. The electrical conductivity of WPU/FGS nanocomposite prepared by in situ polymerization method [61] was also increased up to 10^{15} fold compared to pristine WPU. This is due to the homogeneous dispersion of FGS particles in the WPU matrix and the formation of a conducting network throughout WPU cause an abrupt change in electrical conductivity. Here the percolation threshold was obtained at 2 wt% FGS loading. FGS can be used

to improve the electrical conductivity of WPU as effectively as that of CNTs. The percolation threshold observed for PVDF were 2 wt% FGS and 5 wt% EG loading respectively and these nanocomposites were prepared by solution processing and compression molding method [30]. The higher aspect ratio of FGS compared to EG, makes better conductive network leading to a lower percolation threshold. Polycarbonate composites reinforced with graphite and FGS produced by melt compounding also results in high electrical conductivity with lower percolation threshold for FGS than graphite [62].

3.3 Effect of Filler Modification

There are two factors limiting the application of graphene based polymer composites, i.e. (1) poor dispersion of graphene in the given matrix due to their high specific surface area and strong intermolecular interactions between graphene sheets (2) at low filler content, graphene sheets are covered by polymer chains and thus difficult to achieve the percolation. These issues can be solved by the modification of graphene which impart the desired properties to the platelets. Generally covalent or noncovalent functionalization is employed to increase the effective dispersion of graphene sheets within the polymer. It is established that the chemical functionalization facilitates the dispersion, stabilize graphene and prevent agglomeration [63, 64]. The functional groups attached to graphene can be small molecules or sometimes large polymer chains. The chemical functionalization of graphene is particularly attractive as it can improve the solubility and processability as well as enhance the interactions with organic polymers [65]. Amination, esterification [65], isocyanate modification [66] and polymer wrapping were used in the literature for the functionalization. The electrochemical modification of graphene using ionic liquids has also been reported [67]. Other than the covalent [65, 66] and non covalent modifications [68], other methods such as reduction of GO in a stabilized medium [69], nucleophilic substitution to epoxy groups [70], and diazonium salt coupling [71] are also being practiced.

A homogeneous aqueous suspension of chemically modified graphene in water by means of strong base reduction of graphite oxide in a stabilization medium is reported by Park et al. [69]. Electrostatic stabilization used by Li et al. [72] enables the development of a facile approach to the large scale production of aqueous graphene dispersions. The different surface modifying agents like organic amines, alkyl lithium reagents, isocyanates, and diisocyanate compounds reduce the hydrophilic character of GO sheets by forming amide and carbamate ester bonds with the carboxyl and hydroxyl groups, respectively [66]. Graphite fluoride with alkyl lithium reagents were used for preparation of soluble graphene layers with covalent attachment of alkyl chains to the graphene layers [73].

In another work, the two dimensional GO was modified by isocyanation and dispersed in PS using compression molding and a low percolation threshold at 0.1 vol% was achieved [48]. This value was about 3 times lower than that obtained

for other fillers. The reasons for this high electrical conductivity is attributed to the high aspect ratio of the graphene sheets and their homogenous dispersion in PS as that reported for epoxy/graphene composites [3]. Conductivity of these composites satisfied the approximately 0.15 vol% loading of the antistatic criterion $(10^{-6}$ S m$^{-1})$ for the films. The value increased rapidly over a 0.4 vol% range and at 2.5 vol% loading, the electrical conductivity of composites showed ~0.1 to ~1 S m^{-1}. GNP also enhances the electrical conductivity as seen in its PS composite where 0.38 vol% GNP enhance the value to 5.77 S m^{-1} [46]. Eda et al. prepared PS/FGS composite thin films by [74] a solution blending method and the films exhibited a semi conducting and ambipolar behavior. These composites thin films were electrically conducting with a conductivity ranging from 1 to 24 S m^{-1}.

The electrical conductivity of Poly Aniline (PANI), PANI/GO and PANI/graphene prepared using the chemically modified graphene and PANI nano fibre by in situ polymerization of aniline monomer in the presence of GO under acidic conditions were reported to be 10.6, 23.12 and 168.7 S m^{-1} respectively. The conductivity of PANI/graphene composites was slightly lower than that of the PANI/GO composites, probably due to decrease in the degree of doping in PANI and a change in the morphology of the composite during the reduction, reoxidation and reprotanation processes [75].

Figure 10 [3] shows the plot of the electrical conductivity σ_c of chemically reduced graphene oxide (CRGO)/Polystyrene composites as a function of filler volume fraction φ. It can be seen that in situ CRGO/PS composites exhibit a typical percolation behavior and the introduction of CRGO to PS increase the conductivity to higher than 10 orders of magnitude. Percolation in the composites occurs when the filler concentration is near 0.1 vol%. At 1 vol% CRGO loading, the composite has a conductivity of ~0.1 S m^{-1}. The right and left insets respectively show the plot of log σ_c against log$(\varphi - \varphi_c)$ with φ_c the percolation threshold and the four probe setup for measurements with the computed distributions of the current density (contour lines) with directions and magnitude (arrows).

Fig. 10 Electrical conductivity of insitu CRGO/PS composites as a function of filler volume fraction [3]. Copyright 2012. Reproduced with permission from John Wiley & Sons
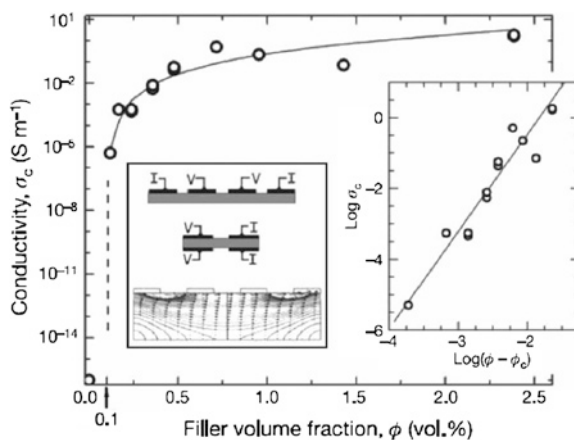
In another work by Chen et al. the electrical properties of both CRGO and thermally reduced graphene oxide (TRGO)/Poly dimethyl siloxane (PDMS) composites observed are much lower than CVD graphene/PDMS composites [76]. They directly synthesized three-dimensional graphene by template directed CVD, in which an interconnected flexible network of graphene exist as the fast transport channel of charge carriers for high electrical conductivity. Even with 0.5 wt% of graphene loading, the PDMS composite shows a very high electrical conductivity of 1,000 S m^{-1}, which is much higher than CRGO and TRGO/PDMS. This good conductivity with a low graphene loading is mainly due to the high electrical conductivity of CVDG and the interconnected 3D network structure in which all the graphene sheets are in direct contact with one another without breaks.

Xu et al. [77] modified graphene via the covalent attachment of a porphyrin ring on the GO surfaces. Thionyl chloride was used to activate the carboxylic acid group in the presence of porphyrin using DMF. Organic isocyanates were used for graphene modification by DMF solvent with methylene chloride and these isocyanate compound was attached to the hydroxyl and carboxyl groups of GO via the formation of carbamate and amide functionalities [66]. The lowest percolation occurred at 0.1 vol% in situ of CRGO reported by Stankovich et al. [68] is attributed to the excellent homogeneous dispersion with solution phase mixing of exfoliated phenyl isocyanate-treated GO sheets with PS.

Modification of graphene was also done by nucleophilic substitution in which aliphatic amine was used to modify GO [68] and the substitution occurs on the epoxy groups of GO and grafting was completed at room temperature [70]. For long chain aliphatic amines (octadecylamine), the reaction mixture was heated under reflux for 24 h. These modified GO derivatives were dispersed more easily in organic solvents. Bourlinos et al. [70] also used an alkaline solution of amino acids was used to modify GO. Nucleophilic attack of the –NH$_2$ end group on the epoxide groups of GO suggests a flat orientation of the amino acid molecules in the interlayer zone of GO. Dodecyl benzene sulfonate was used in reduction of GO with hydrazine and functionalized by a treatment with aryl diazonium salts [71]. Epitaxial graphene grown on SiC wafers were modified chemically with aryl groups via the formation of covalent bonds to the conjugated carbon atoms [78]. Electrochemical modification is also employed for graphene where graphite is electrochemically treated to produce a colloidal suspension of chemically modified graphene. The pyrene treatment done on graphene by Kim et al. reveals the capability of polycyclic aromatic hydrocarbon, pyrene/perylene to adsorb strongly on the graphene surface through π–π interactions [79]. As a result the conductivity was significantly improved.

Since ultrasonic treatment failed to achieve a good dispersion of graphene in water soluble polymer in the presence of surfactants, polymeric anions were used in the reduction which results the stable aqueous dispersion polymer-grafted dispersion of graphene [80]. High quality water soluble and organic solvent soluble graphene sheets for a range of applications were obtained from EG using 7,7,8,8-tetracyanoquinodimethane (TCNQ) anion as a stabilizer [81]. Water soluble pyrene derivative,1-pyrenebutyrate (PB) also acted as a stabilizer for the preparation of aqueous dispersions of graphene sheets [82].

3.4 Other Factors

In addition to the three factors discussed in the previous sub sections, several miscellaneous points also influence electrical conductivity of graphene and its derivative filled polymers. Zhang and co-workers [80] studied the effect of oxygen content on graphene sheets on the electrical property of graphene-PMMA nanocomposites. The percolation threshold increased with increasing oxygen content and the composite with lowest oxygen content (graphene-13.2) show a dramatic increment in electrical conductivity of over 12 orders of magnitude, from 3.33×10^{-14} S m^{-1} with 0.4 vol% of graphene to 2.38×10^{-2} S m^{-1} with 0.8 % of graphene. At 2.67 vol% the electrical conductivity reached up to 10 S m^{-1} indicating interconnected graphene network. Moreover the composite with lowest oxygen content exhibited much higher conductivity, in the percolation transition range than composites with higher content of oxygen (graphene-9.6 and graphene-5.0). The presence of oxygen-containing groups on graphene has been proved to disrupt its graphitic sp^2 network and decrease its intrinsic conductivity leading to a final conclusion that the higher the oxygen content, the lower the intrinsic conductivity.

Orientation of graphene platelets in polymer is another factor influencing composite conductivity. When graphene sponge containing randomly distributed graphene sheets are added to epoxy (insulator with conductivity around at 10^{-13} S cm^{-1}) [83] the magnitude of conductivity increased 12 times attributed to the compactly interconnected graphene network constructed within the polymer. Further improvement was also noticed upon graphene sponge treatment [84]. The filler surface area is yet another factor which causes the conductivity variation as noticed in the case of PVA/RGO nanocomposites [85]. Both large area (LRGO) and small area RGOs (SRGO) were used to fabricate the nanocomposites and found higher electrical conductivity for PVA/LRGO than that of SRGO at the same filler content. Percolation happened at 0.189 wt% of filler. The conductivity increased with specific surface area as well as with the reduction temperature. Conductivity improves when thermal reduction temperature exceeds critical temperature. Also high temperature is more efficient for reducing the GO sheets than low temperature. The electrical conductivity increased to the highest value at the reduction temperature 200 °C which indicating that the critical temperature for the thermal reduction in PVA/GO system is 200 °C. Swelling was also employed to understand the mechanism involved and found a decrease in conductivity after swelling due to the destroyed conductive networks. During swelling, water molecules interact between the RGO sheets and destroy the electrical networks and the conductivity is lower for PVA/LRGO than PVA/SRGO nanocomposites after swelling. This indicates easy destruction of the SRGO network after treatment [85].

Thermal reduction is an efficient way to produce the nanocomposite with low percolation threshold and high electrical conductivity and also it's suitable for preparing the thermoset or thermoplastic polymer/RGO nanocomposites through reduction of GO sheets at appropriate temperature. The long reduction time improves the electrical conductivity of nanocomposites [85]. It is reported that thermally reduced

GO has higher electrical conductivity than chemically reduced GO due to the absence of oxygenated functional groups in TRGO [45, 46]. This effect of thermal and chemical reduction of GO on the electrical properties of graphene/PU composites was studied by Kim et al. [53]. The electrical properties of graphene and graphite in terms of conductivity or sheet resistance can be modulated by controlling the number of graphene layers [86]. For this purpose, the sheet resistance values were checked for graphene and graphite films containing different numbers of layers. The sheet resistance was reduced by a factor of approximately 25 as the number of layers increased from 24 to 850 layers. Additionally, the current versus back-gate characteristics showed much stronger modulation in 24-layer graphene compared with a negligible change in the thick graphite (850 layers) due to the stronger screening effect as the number of layers increases. The low sheet resistance and field-effect response of graphite are advantageous for applications in conductive films or electrodes. In contrast, the superior transconductance level of the 24-layer graphene is appropriate for the active channels of field-effect transistors (FETs).

On the basis of the above results, we can conclude that many factors including filler aspect ratio, surface area, concentration, dispersion state, mode of synthesis and contact resistance are key factors affecting the electrical properties of graphene/polymer composites.

4 Applications

Based on this chapter, it is clear that the reinforcement of graphene and its polymer nanocomposites have shown very promising results in enhancing the electrical conductivity at low percolation threshold. The discovery of graphene as nanofiller has opened a new dimension for the production of light weight, low cost, and high performance composite materials for a range of applications. The electrically conductive polymer/graphene nanocomposites have been widely used for making various sensors, memory and energy storage, antistatic coatings, EMI etc. and have potential applications in the biomedical fields, such as ultraminiaturized low cost sensors for the analysis of blood and urine. Moreover the polymer/graphene flexible electrode has some commercial applications in LEDs, transparent conducting coatings for solar cells and displays.

5 Conclusion

The development of a nanolevel dispersion of graphene particles in a polymer matrix has opened a new and interesting area in materials science in recent years. Its unique properties make it suitable to improve the electrical properties of polymer composites. This chapter summarizes the electrical properties of various polymer/graphene composites and the different factors affecting electrical

conductivity. We discussed the percolation threshold based on filler volume fraction, processing methods, aspect ratio, surface area, orientation etc. In order to improve conductivity, the dispersion of graphene in polymer matrices and the graphene–polymer interaction needs to be improved, which are achieved by the surface modification of graphene. Finally a few electronic applications of these high-performance graphene composite materials is mentioned.

References

1. Huang X, Yin Z, Wu S, Qi X, He Q, Zhang Q, Yan Q, Boey F, Zhang H (2011) Graphene-Based Materials: Synthesis, Characterization, Properties, and Applications. Small 7: 1876–1902.
2. Dong L X, Chen Q (2010) Properties, synthesis, and characterization of grapheme. Frontiers of Materials Science in China 4: 45–51.
3. Du J, Cheng H M (2012) The Fabrication, Properties, and Uses of Graphene/Polymer Composites. Macromolecular Chemistry and Physics 213: 1060–1077.
4. Cai W W, Piner R D, Stadermann F J, Park S, Shaibat M A, Ishii Y, Yang D X, Velamakanni A, An S J, Stoller M, An J H, Chen D M, Ruoff R S S (2008) Synthesis and solid-state NMR structural characterization of C-labeled graphite oxide. Science 321: 1815–1817.
5. Li X S, Cai W W, An J H, Kim S, Nah J, Yang D X, Piner R, Velamakanni A, Jung I, Tutuc E, Banerjee S K, Colombo L, Ruoff R S (2009) Large-area synthesis of high-quality and uniform graphene films on copper foils. Science 324: 1312–1314.
6. Novoselov K S, Geim A K, Morozov S V, Jiang D, Zhang Y, Dubonos S V, Grigorieva I V, Firsov A A (2004) Electric field effect in atomically thin carbon films. Science 306: 666–669.
7. Novoselov K S, Geim A K, Morozov S V, Jiang D, Katsnelson M I, Grigorieva I V, Dubonos S V, Firsov A A (2005) Two-dimensional gas of massless Dirac fermions in grapheme. Nature 438: 197–200.
8. Zhang Y, Tan Y W, Stormer H L, Kim P (2005) Experimental observation of the quantum Hall effect and Berry's phase in grapheme. Nature 438: 201–204.
9. Geim A K, Novoselov K S (2007) The rise of graphene. Nature Mater 6: 183–191.
10. Dreyer D R, Ruoff R S, Bielawski C W (2010) From conception to realization: an historial account of graphene and some perspectives for its future. Agnewandle Chemie International Edition 49: 9336–9345.
11. Boehm H P, Setton R, Stumpp E (1986) Nomenclature and terminology of graphite intercalation compounds. Carbon 24: 241–245.
12. Novoselov K S, Jiang D, Schedin F, Booth T, Khotkevich V V, Morozov S V, Geim A K (2005) Two-dimensional atomic crystals. Procedings of the National Academy of Sciences 102: 10451–10453.
13. Park S, Ruoff R S (2009) Chemical methods for the production of graphenes. Nature Nanotechnology 4: 217–224.
14. Fujita D, Yoshihara K(1994) Surface precipitation process of epitaxially grown graphite (0001) layers on carbon-doped nickel(III) surface. J Vac Sci Technol A 1994, 12, 2134–2139.
15. Gao J H, Fujita D, Xu M S (2010) Unique synthesis of few-layer grapheme films on carbon-doped $Pt_{83}Rh_{17}$ surfaces. ACS Nano 4: 1026–1032.
16. Xu M S, Fujita D, Chen H Z, Hanagata N(2011) Formation of monolayer and few-layer hexagonal boron nitride nanosheets via surface segregation. Nanoscale 3: 2854–2858.
17. Fujita D (2011) Nanoscale synthesis and characterization of graphene-based objects. Science and Technology of Advanced Materials 12: 044611 (1–10).
18. Xu M S, Fujita D, Sagisaka K, Watanable E, Hanagata N (2011) Production of extended single-layer graphene. ACS Nano 5: 1522–1528.

19. Xu M S, Endres R G, Tsukamoto S, Kitamura M, Ishida S, Arakawa Y (2005) Conformation and local environment dependent conductance of DNA molecules. Small 1: 1168–1172.

20. Xu M S, Tsukamoto S, Ishida S, Kitamura M, Arakawa Y, Endres R G, Shimoda M (2005) Conductance of single thiolated poly(GC)-poly(GC) DNA molecules. Applied Physics Letters 87: 083902 (1–3).

21. Merino P, Svec M, Pinardi A L, Otero G, Martin-Gago J A (2011) Strain-driven moiré super-structures of epitaxial graphene on transition metal surfaces. ACS Nano 5: 5627–5634.

22. Zhou S X, Zhu Y, Du H D, Li B H, Kang F Y (2012) Preparation of oriented graphite/poly-mer composite sheets with high thermal conductivities by tape casting. New Carbon Mater 27: 241–249.

23. Zhou S, Chiang S, Xu J, Du H, Li B, Xu C, Kang F (2012) Modeling the in-plane thermal conductivity of a graphite/polymer composite sheet with a very high content of natural flake graphite. Carbon 50: 5052–5061.

24. Zhang W, Xu H, Chen Y, Cheng S, Fan L (2013) Polydiacetylene-polymethylmethacrylate/graphene composites as one-shot, visually observable, and semiquantative electrical current sensing materials. ACS Applied Materials & Interfaces 5: 4603–4606.

25. Gudarzi M M, Sharif F (2012) Enhancement of dispersion and bonding of graphene-polymer through wet transfer of functionalized graphene oxide. Express Polymer Letters 6: 1017–1031.

26. Yu H Y, Xu M Q, Yu S H, Zhao G C (2013) A novel non-enzymatic glucose sensor based on CuO - graphene nanocomposites. International Journal of Electrochemical Science 8: 8050–8057.

27. Paszkiewicz S, Szymczyk A, Spitalsky S, Soccio M, Mosnacek J, Ezquerra T A, Roslaniec Z (2012) Electrical conductivity of poly(ethylene terephthalate)/expanded graphite nano-composites prepared by in situ polymerization. Journal of Polymer Science Part B: Polymer Physics 50: 1645–1652.

28. Wei H, Zhu J, Wu S, Wei S, Guo Z (2013) Electrochromic polyaniline/graphite oxide nano-composites with endured electrochemical energy storage. Polymer 54: 1820–1831.

29. Chen G L, Shau S M, Juang T Y, Lee R H, Chen C P, Suen S Y, Jeng R J (2011) Single-layered graphene oxide nanosheet/polyaniline hybrids fabricated through direct molecular exfoliation. Langmuir 27: 14563–14569.

30. Ansari S, Emmanuel P G (2009) Functionalized graphene sheet-poly(vinylidene fluo-ride) conductive nanocomposites. Journal of Polymer Science Part B: Polymer Physics 47: 888–897.

31. Chandra S, Bag S, Das P, Bhattacharya D, Pramanik P (2012) Fabrication of magnetically separable palladium–graphene nanocomposite with unique catalytic property of hydrogena-tion. Chemical Physics Letters 519: 59–63.

32. Matusinovic Z, Rogosic M, Sipusic J (2009) Synthesis and characterization of poly(styrene-co-methyl methacrylate)/layered double hydroxide nanocomposites via in situ polymeriza-tion. Polymer Degradation and Stability 94: 95–101.

33. Aldosari M, Othman A, Alsharaeh E (2013) Synthesis and characterization of the in situ bulk polymerization of PMMA containing graphene sheets using microwave irradiation. Molecules 18: 3152–3167 (3).

34. Nuvoli D, Alzari V, Sanna R, Scognamillo S, Piccinini M, Peponi L, Kenny J M, Mariani A (2012) The production of concentrated dispersions of few-layer graphene by the direct exfo-liation of graphite in organosilanes. Nanoscale Research Letters 7: 674 (1–7).

35. Wu W, Liu Z, Jauregui L A, Yu Q, Pillai R, Cao H, Bao J, Chen Y P, Pei S S (2010) Wafer-scale synthesis of graphene by chemical vapor deposition and its application in gas sensing. Sensors and Actuators B 150: 296–300.

36. Wang Y, Yang R, Shi Z, Zhang L, Shi D, Wang E, Zhang G (2011) Super-elastic graphene ripples for flexible strain sensors. ACS Nano 5: 3645–3650.

37. Sojoudi H, Graham S (2013) Transfer-free selective area synthesis of graphene using solid-state self-segregation of carbon in Cu/Ni bilayers. ECS Journal of Solid State Science and Technology 2: M17–M21.

38. Kim K S, Zhao Y, Jang H, Lee S Y, Kim J M, Kim K S, Ahn J H, Kim P, Choi J Y, Hong B H (2009) Large-scale pattern growth of graphene films for stretchable transparent electrodes. Nature 457: 706–710.

39. Reina A, Jia X T, Ho J, Nezich D, Son H B, Bulovic V, Dresselhaus M S, Kong J (2009) Large area, few-layer graphene films on arbitrary substrates by chemical vapor deposition. Nano Letters 9: 30–35.

40. Berciaud S, Ryu S, Brus L E, Heinz T F (2009) Probing the intrinsic properties of exfoliated graphene: Raman spectroscopy of free-standing monolayers. Nano Letters 9: 346–352.

41. Cao H, Yu Q, Jauregui L A, Tian J, Wu W, Liu Z, Jalilian R, Benjamin D K, Jiang Z, Bao J, Pei S S, Chen Y P (2010) Electronic transport in chemical vapor deposited graphene synthesized on Cu: quantum Hall effect and weak localization. Applied Physics Letters 96: 122106 (1–3).

42. Ferrari A C, Meyer J C, Scardaci V, Casiraghi C, Lazzeri M, Mauri F S, Piscanec F S, Jiang D, Novoselov K S, Roth S, Geim A K (2006) Raman spectrum of graphene and graphene layers. Physical Review Letters 97: 187401 (1–4).

43. Peng Xu, James Loomis, and Balaji Panchapakesana. load transfer and mechanical properties of chemically derived single layer graphene reinforcements in polymer composites. Nanotechnology. 2012 December 21; 23(50): 505713

44. Mohiuddin T M G, Lombardo A, Nair R R, Bonetti A, Savini G, Jalil R, Bonini N, Basko D M, Galiotis C, Marzari N, Novoselov K S, Geim A K, Ferrari A C (2009) Uniaxial strain in graphene by Raman spectroscopy: G peak splitting, Grüneisen parameters, and sample orientation. Physical Review B 79: 205433.

45. Galpaya D, Wang M, Liu M, Motta N, Waclawik E, Yan C (2012) Recent advances in fabrication and characterization of graphene-polymer nanocomposites. Graphene 1: 30–49

46. Kuilla T, Bhadrab S, Yao D, Kim N H, Bose S, Lee J H (2010) Recent advances in graphene based polymer composites. Progress in Polymer Science 35: 1350–1375

47. Xie S H, Liu Y Y, Li J Y (2008) Comparison of the effective conductivity between composites reinforced by graphene nanosheets and carbon nanotubes. Applied Physics Letters 92 : 243121 (1–3).

48. Stankovich S, Dikin D A, Dommett G H B, Kohlhaas K M, Zimney E J, Stach E A, Piner R D, Nguyen S T, Ruoff R S (2006) Graphene-based composite materials. Nature 442: 282–286.

49. Alamusi N H, Hisao F, Satoshi A, Yaolu L, Jinhua L (2011) Piezoresistive strain sensors made from carbon nanotubes based polymer nanocomposites. Sensor 11: 10691–10723.

50. Liang J J, Wang Y, Huang Y, Ma Y, Liu Z, Cai J, Zhang C, Gao H, Chen Y (2009) Electromagnetic interference shielding of graphene/epoxy composites. Carbon 47: 922–925.

51. Pang H, Chen T, Zhang G, Zeng B, Li Z M (2010) An electrically conducting polymer/graphene composite with a very low percolation threshold. Materials Letters 64: 2226–2229.

52. Zhang H B, Zheng W G, Yan Q, Yang Y, Wang J W, Lu Z H, Ji G Y, Yu Z Z (2010) Electrically conductive polyethylene terephthalate/graphene nanocomposites prepared by melt compounding. Polymer 51: 1191–1196.

53. Kim H, Y. Miura Y, Macosko C W (2010) Graphene/Poly- urethane Nanocomposites for Improved Gas Barrier and Electrical Conductivity. Chemistry of Materials 22: 3441–3450.

54. Maiti S, Shrivastava N K, Suin S, Khatua B B (2013) Polystyrene/MWCNT/graphite nanoplate nanocomposites: efficient electromagnetic interference shielding material through graphite nanoplate–MWCNT–graphite nanoplate networking. ACS Applied Materials & Interfaces 5: 4712–4724.

55. Zhang H B, Zheng W G, Yan Q, Yang Y, Wang J W, Lu Z H, Ji G Y, Yu Z Z (2010) Electrically conductive polyethylene terephthalate/graphene nanocomposites prepared by melt compounding. Polymer 51: 1191–1196.

56. Liang Y, Gholamerza P, Seyed A Monemian, Ica M Zioczowe (2014) Epoxy composites with carbon nanotubes and graphene nanoplatetletes-dispersion and synergy effects. Carbon 78: 268–278.

57. He L, Tjong S C (2013) Low percolation threshold of graphene/polymer composites prepared by solvothermal reduction of graphene oxide in the polymer solution. Nanoscale Research Letters 8: 132 (1–7).

58. Nan C W, Shen Y, Ma J (2010) Physical properties of composites near percolation. Annual Review of Materials Research 40: 131–151.
59. Cui L L, Lu X F, Chao D M, Liu H T, Li Y X, Wang C (2011) Graphene-based composite materials with high dielectric permittivity via an in situ reduction method. physica status solidi (a) 208: 459–461.
60. Hu H, Wang X, Wang J, Wan L, Liu F, Zheng H, Chen R, Xu C (2010) Preparation and properties of graphene nanosheets-polystyrene nanocomposites via in situ emulsion polymerization. Chemical Physics Letters 484 : 247–253.
61. Lee Y R, Raghu A V, Jeong H M, Kim B K (2009) Properties of waterborne polyurethane/functionalized graphene sheet nanocomposites prepared by an in situ method. Macromolecular Chemistry and Physics 210 : 1247–1254.
62. Kim H, Macosko C W (2009) Processing–property relationships of polycarbonate/ graphene nanocomposites. Polymer 50:3797– 3809.
63. Geng Y, Wang S J, Kim J K (2009) Preparation of graphite nanoplatelets and graphene sheets. Journal of Colloid and Interface Science 336 : 592–598.
64. Wei T, Luo G, Fan Z, Zheng C, Yan J, Yao C, Li W, Zhang C (2009) Preparation of graphene nanosheet/polymer composites using in situ reduction-extractive dispersion. Carbon 47:2296–2299.
65. Niyogi S, Bekyarova E, Itkis M E, McWilliams J L, Hamon M A, Haddon R C (2006) Solution properties of graphite and graphene. Journal of American Chemical Society 128:7720–7721.
66. Stankovich S, Piner R D, Nguyen S T, Ruoff R S (2006) Synthesis and exfoliation of isocyanate-treated graphene oxide nanoplatelets. Carbon 44:3342–3347.
67. Liu N, Luo F, Wu H, Liu Y, Zhang C, Chen J (2008) One step ionic-liquid assisted electrochemical synthesis of ionic-liquid-functionalized graphene sheets directly from graphene. Advanced Functional Materials 18:1518–1525.
68. Stankovich S, Piner R D, Chen X, Wu N, Nguyen S T, Ruoff R S (2006) Stableaqueous dispersions of graphitic nanoplatelets via the reductionof exfoliated graphite oxide in the presence of poly(sodium 4-styrenesulfonate). Journal of Materials Chemistry 16:155–158.
69. Park S, An J, Piner R D, Jung I, Yang D, Velamakanni A, Nguyen S T, Ruoff R S (2008) Aqueous suspension and characterization of chemically modified grapheme sheets. Chemistry of Materials 20:6592–6594.
70. Bourlinos A B, Gournis D, Petridis D, Szabo T, Szeri A, Dekany I (2003) Graphite oxide: chemical reduction to graphite and surface modificationwith primary aliphatic amines and amino acids. Chemistry of Materials 19: 6050–6055.
71. Lomeda J R, Doyle C D, Kosynkin D V, Hwang W F, Tour J M (2008) Diazonium functionalization of surfactant-wrapped chemically converted graphene sheets. Journal of American Chemical Society 130:16201–16206.
72. Li D, Muller M B, Gilje S, Kaner R B, Wallac G G (2007) Processable aqueous dispersions of graphene nanosheets. Nature Nanotechnology 3:101–105.
73. Worsley K A, Ramesh P, Mandal S K, Niyogi S, Itkis M E, Haddon R C (2007) Soluble graphene derived from graphite fluoride. Chemical Physics Letters 445: 51–56.
74. Eda G, Chhowalla M (2009) Graphene-based composite thin films for electronics. Nano Letters 9: 814–818.
75. Bhadra S, Khstagir D, Singh A K, Lee J H (2009) Progress in preparation, processing and applications of polyaniline. Progress in Polymer Science 34:783–810.
76. Chen Z, Ren W, Gao L, Liu B, Pei S, Cheng H M (2011) Three-dimensional flexible and conductive interconnected graphene networks grown by chemical vapour deposition. Nature Materials 10: 424–428.
77. Xu Y, Liu Z, Zhang X,Wang Y, Tian J, Huang Y (2009) A graphene hybrid material covalently functionalized with porphyrin: synthesis and optical limiting property. Advanced Mater 21: 1275–1279.

78. Berger C, Song Z, Li T, Li X, Ogbazghi AY, Feng R (2004) Ultrathin epitaxial graphite: 2D electron gas properties and a route toward graphene-based nanoelectronics. Journal of Physics and Chemistry B 108:19912–19916.
79. Kim SC, Lee H, Jeong HM (2010) Effect of pyrene treatment on the properties of graphene/epoxy nanocomposites. Macromolecular Research 18(11): 1125–1128.
80. Zhang H B, Zheng W G, Yan Q, Yang Y, Wang J W, Lu Z H, Ji G Y, Yu Z Z (2010) Electrically conductive polyethylene terephthalate/graphene nanocomposites prepared by melt compounding. Polymer 51:1191–1196.
81. Hao R, Qian W, Zhang L, Hou Y (2008) Aqueous dispersions of TCNQ-anion stabilized graphene sheets. Chem Commun 48: 6576–6578.
82. Xu Y, Bai H, Lu G, Li C, Shi G (2008) Flexible graphene films via the filtration of water-soluble noncovalent functionalized graphene sheets. Journal of American Chemical Society 130:5856–5857.
83. Wang T X, Liang G Z, Yuan L, Gu A (2014) Unique hybridized graphene and its high dielectric constant composites with enhanced frequency stability, low dielectric loss and percolation threshold. Carbon 77: 920–932.
84. Li Y, Samad Y A, Polychronopoulou K, Alhassan S M, Liao K (2014) Highly Electrically Conductive Nanocomposites Based on PolymerInfused Graphene Sponges. Scientific Reports 4:4652 (1–6).
85. Zhou T N, Qi X D, Fu Q (2013) The preparation of the poly(vinyl alcohol)/graphene nanocomposites with low percolation threshold and high electrical conductivity by using the large-area reduced graphene oxide sheets. Express Polymer Letters 7: 747–755.
86. Park J U, Nam S W, Lee M S, Lieber C M (2012) Synthesis of monolithic graphene–graphite integrated electronics. Nature Materials 11: 120–125.

Graphene-Based Polymer Nanocomposites in
Electronics
Sadasivuni, K.K.; Ponnamma, D.; Kim, J.; Thomas, S.
(Eds.)
2015, VI, 382 p. 175 illus., 143 illus. in color., Hardcover
ISBN: 978-3-319-13874-9